Journal of Magnetic Resonance 210 (2011) 38–43

Contents lists available at ScienceDirect

Journal of Magnetic Resonance

journal homepage: www.elsevier.com/locate/jmr

Fast fat-suppressed reduced field-of-view temperature mapping using 2DRF excitation pulses

Jing Yuan [a,*], Chang-Sheng Mei [b,c], Bruno Madore [b], Nathan J. McDannold [b], Lawrence P. Panych [b]

[a] Department of Imaging and Interventional Radiology, The Chinese University of Hong Kong, Shatin, New Territories, Hong Kong
[b] Department of Radiology, Brigham and Women's Hospital, Harvard Medical School, Boston, MA, USA
[c] Department of Physics, Boston College, Chestnut Hill, MA, USA

ARTICLE INFO

Article history:
Received 3 January 2011
Revised 2 February 2011
Available online 2 March 2011

Keywords:
2DRF pulse
Fat suppression
Focused ultrasound
Proton resonance frequency
Temperature mapping
Reduced field-of-view

ABSTRACT

The purpose of this study is to develop a fast and accurate temperature mapping method capable of both fat suppression and reduced field-of-view (rFOV) imaging, using a two-dimensional spatially-selective RF (2DRF) pulse. Temperature measurement errors caused by fat signals were assessed, through simulations. An 11 × 1140 μs echo-planar 2DRF pulse was developed and incorporated into a gradient-echo sequence. Temperature measurements were obtained during focused ultrasound (FUS) heating of a fat–water phantom. Experiments both with and without the use of a 2DRF pulse were performed at 3*T*, and the accuracy of the resulting temperature measurements were compared over a range of TE values. Significant inconsistencies in terms of measured temperature values were observed when using a regular slice-selective RF excitation pulse. In contrast, the proposed 2DRF excitation pulse suppressed fat signals by more than 90%, allowing good temperature consistency regardless of TE settings. Temporal resolution was also improved, from 12 frames per minute (fpm) with the regular pulse to 28 frames per minute with the rFOV excitation. This technique appears promising toward the MR monitoring of temperature in moving adipose organs, during thermal therapies.

1. Introduction

Fast and accurate temperature mapping is essential to non-invasive thermal therapies such as MR-guided focused ultrasound (FUS) ablations, to ensure the efficacy and safety of the treatment. Many MR parameters that have temperature dependence have been suggested for temperature mapping using MRI, for example, T_1 relaxation times [1,2], proton density [3], magnetization transfer [4], diffusion coefficient [5] and proton resonance frequency (PRF) [6,7]. PRF-based temperature mapping has received the greatest acceptance due to its higher sensitivity to small temperature changes (0.01 ppm/°C) [8], its linear response over a broad range of temperatures (about −15 °C to 100 °C) [9], and its near-independence on tissue type (except for adipose tissue) and on thermal history [10]. On the other hand, PRF-based temperature measurements can be corrupted by the presence of fat, as the PRF of fat is mostly independent of temperature [11]. In voxels featuring both fat and water, as may be found in the breast or in a diseased fatty liver, the MR signal consists of the complex sum of a water and a fat signal, each one with its own magnitude and phase. In such voxels, the temperature-induced phase changes to the water signal are essentially obscured by the temperature-independent fat signal, leading to underestimated values on temperature measurements [12]. To overcome this problem, fat suppression techniques have to be employed.

In addition to fat-related accuracy problems as described above, MR thermometry also poses significant challenges in terms of imaging performance and imaging speed. Large thermal gradients and rapid temperature changes may be produced during thermal treatment, creating a need for reasonably high spatial and temporal resolution. Possible motion and the need to track targeted lesions may also create high demands in terms of spatial and temporal resolution. Many approaches have been proposed to speed-up the image acquisition process in temperature mapping by the use of fast sequences [13–15] and parallel imaging [16,17].

In the present work, a particular echo-planar two-dimensional RF (2DRF) excitation pulse is proposed to address all at once both the fat-suppression and fast-imaging needs encountered in PRF MR thermometry applications. With regard to fat suppression, an echo-planar 2DRF pulse works in a similar manner as a spatial-spectral (SPSP) pulse [12,18,19], except that blip gradients along the phase-encoding (PE) direction in a 2DRF pulse convert the spectral response of fat into a spatial shift along the PE direction [20]. With regard to fast imaging, a 2DRF pulse can be used to excite only a reduced FOV around the heating focus, allowing

* Corresponding author. Address: Department of Imaging and Interventional Radiology, The Chinese University of Hong Kong, Shatin, New Territories, Hong Kong. Fax: +852 2636 0012.
E-mail address: jyuan@cuhk.edu.hk (J. Yuan).

1090-7807/$ - see front matter © 2011 Elsevier Inc. All rights reserved.
doi:10.1016/j.jmr.2011.02.004

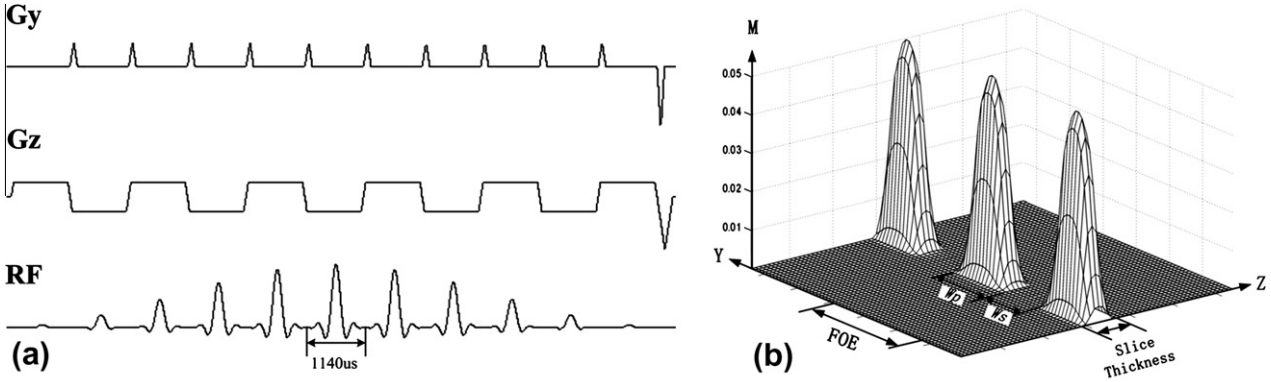

Fig. 1. (a) The waveform of the echo-planar 2DRF pulse used for fat suppression and reduced field-of-view imaging. The 2DRF pulse consists of 11 SINC sub-pulses and the sub-pulse duration is 1140 μs. The amplitude of the sub-pulses is modulated by a Gaussian envelope. (b) The excitation profile obtained using the echo-planar 2DRF pulse features periodic replica along the PE direction.

reductions in the number of acquired phase encodes and a corresponding decrease in scan time. The 2DRF pulses proposed here can fulfill both tasks at once, suppressing fat signals while exciting only a portion of the FOV, for fast imaging. It may be noted that this approach is compatible with different fast imaging sequences and different acceleration methods such as parallel imaging, to further the acquisition speed. The present technique is expected to be especially useful in applications where fat is present and fast imaging may be required, such as for MR guided thermal ablations in breast or diseased fatty liver tissues.

2. Theory

2.1. Fat–water combined system in PRF model

The general theoretical PRF model for a two-component system has been described by Kuroda et al. [21]. Here we focus on the specific fat–water combined two-component system and analyze the measured temperature error due to the presence of fat and its relationship with various factors such as echo time, magnet_field strength and fat content percentage. In general, the signal (S_c) in such a two-component system can be expressed by the sum of water (W) and fat (F) vectors:

$$\vec{S}_c = A_c e^{i\Phi_c} = \vec{W} + \vec{F} = A_w e^{i\Phi_w} + A_f e^{i\Phi_f}, \tag{1}$$

where A_w, A_f and A_c represent the amplitude of the water, fat, and fat–water combined signal, respectively, while Φ_w, Φ_f and Φ_c represent the corresponding phases. In the PRF model, the measured temperature change (ΔT_m) is proportional to the phase variation ($\Delta\Phi_c$) during the thermal treatment, and is expressed as:

$$\Delta T_m = \frac{\Delta\Phi_c}{\gamma\cdot\alpha\cdot B_0\cdot \mathrm{TE}} = \frac{\Phi_{c1}-\Phi_{c0}}{\gamma\cdot\alpha\cdot B_0\cdot \mathrm{TE}}, \tag{2}$$

where Φ_{c1} and Φ_{c0} are the combined signal phase at the current image and the baseline reference respectively, γ is the gyromagnetic ratio, α is the PRF change coefficient (0.01 ppm/°C), B_0 is the main magnetic field strength and TE is the sequence echo time. Φ_{c0} and Φ_{c1} can be calculated as in Eqs. (3) and (4), respectively:

$$\Phi_{c0} = \tan^{-1}\left(\frac{A_w\sin\Phi_{w0}+A_f\sin\Phi_{f0}}{A_w\cos\Phi_{w0}+A_f\cos\Phi_{f0}}\right), \tag{3}$$

$$\Phi_{c1} = \tan^{-1}\left(\frac{A_w\sin(\Phi_{w0}+\Delta T\cdot\gamma\cdot\alpha\cdot B_0\cdot \mathrm{TE})+A_f\sin\Phi_{f0}}{A_w\cos(\Phi_{w0}+\Delta T\cdot\gamma\cdot\alpha\cdot B_0\cdot \mathrm{TE})+A_f\cos\Phi_{f0}}\right),$$
$$\text{with}\quad \Phi_{f0} = \Phi_{w0} + 2\pi\cdot\Delta f\cdot \mathrm{TE}. \tag{4}$$

In Eq. (4), ΔT is the true temperature change, Δf is the offset frequency of fat at B_0, and the subscripts in Eqs. (3) and (4) have the same meaning as in Eq. (1). Because the phase of the fat signal is independent of temperature, the presence of fat leads to the phase modulation of the combined system and a temperature measurement error of $\delta T = \Delta T_m - \Delta T$.

3. 2DRF Pulses and rFOV

A small-tip-angle model [22] was used for the echo-planar 2DRF pulse design in this study.

An echo-planar 2DRF (Fig. 1a) pulse follows a Cartesian trajectory in excitation k-space. The gradient blips (Gz) convert spectral shift into a spatial shift along the PE (y) direction, and the SINC sub-pulses and gradients Gz select a slice in the z direction.As seen in Fig. 1b, the 2DRF excitation profile replicates periodically along the PE direction according to the Nyquist theorem. The excitation profile thickness, the distance between two neighboring excitations and the unexcited region are referred to as the passband width (W_p), field of excitation (FOE), and stopband width (W_s), respectively. The FOE and passband width can be expressed as:

$$\mathrm{FOE} = W_p + W_s = \frac{1}{a_{blip}}, \tag{5}$$

$$W_p = \frac{\mathrm{TBW}}{(n-1)a_{blip}} = \frac{\mathrm{TBW}}{(n-1)}\mathrm{FOE}, \tag{6}$$

where a_{blip} is the area of a Y blip gradient, n is the number of sub-pulses and TBW is the time-bandwidth product of the modulation envelop waveform.

Fat signals experience a relatively large spatial shift ΔS along the PE direction, which can be expressed as:

$$\Delta f = \frac{a_{blip}}{T_{sub}}\cdot(r-r_0) = \frac{1}{T_{sub}}\cdot\frac{\Delta r}{\mathrm{FOE}}\prime, \quad \Delta r = \Delta f\cdot T_{sub}\cdot\mathrm{FOE}, \tag{7}$$

where Δf is the frequency offset for fat and T_{sub} represents the sub-pulse duration.To achieve fat suppression, the fat profile Δr must be shifted by $\Delta r \geqslant W_p$. Meanwhile, $W_s \geqslant W_p$ is required to enable rFOV imaging without aliasing artifacts [20]. When the fat profile shift Δr is equal to half the FOE (corresponds to T_{sub} = 1140 μs at 3T for the fat offset frequency of 440 Hz), a maximum FOV reduction factor of W_s/W_p can be achieved.

4. Methods

4.1. Simulations

A numerical program using MATLAB v7.0 (MathWorks, Natick, MA) was developed to simulate the effects of the fat component on temperature measurements, in the PRF model. The fat percentage is defined as the ratio of the bulk amplitude of the complex fat signal to that of the water, i.e., A_f/A_w.

4.2. MRI scans and temperature mapping

A 2DRF pulse with 11 sub-pulses, each one 1140 μs in duration (see Fig. 1), was implemented to enable both fat-suppression and rFOV imaging. The 2DRF excitation FOE and profile spatial shift can be controlled through adjustments in blip gradient strength and RF phase for each sub-pulse, through user-defined parameters [20]. All experiments were performed on a 3*T* GE Signa MRI scanner (General Electric Healthcare, Milwaukee, WI). A fat-suppressed rFOV excitation pattern was first demonstrated without heating, on a phantom consisting of separated vegetable oil and water with a circular cross section with a radius of around 8 cm (Imaging parameters: TE: 17 ms, TR: 34 ms, flip angle: 30°, receiver bandwidth (BW): ±8.06 kHz, matrix: 192 × 192, FOV: 10 cm, and slice thickness: 5 mm).

For experiments with heating, the ultrasonic energy was generated by a single-element, spherically curved, piezoelectric transducer (radius of curvature = 100 mm and diameter = 100 mm) with a resonance frequency of 1.5 MHz, driven by a function generator (Model 396, Fluke, Everett, WA) and RF amplifier (model 240L, E and I, Rochester, NY). RF power was monitored using a power meter (model 438A, Hewlett Packard, Palo Alto, CA) and dual directional coupler (model C1373, Werlatone, Brewster, NY). The transducer produced an ellipsoid focal spot whose half-maximum intensity length and diameter were 10 mm and 5 mm, respectively. A cheese phantom (10 cm × 4 cm × 4 cm in size) containing a homogeneous mixture of fat and water (Original Velveeta, 21% fat, Kraft Foods Inc., Northfield, IL) was heated for 30 s using the transducer (acoustic power: 6 W). Sonication began following an initial baseline scan, and a time-series of rFOV images were acquired during heating and cooling using a modified fast gradient-echo sequence (FGRE) and the 11 × 1140 μs 2DRF pulse for excitation (TR: 40 ms, flip angle: 30°, BW: 8.06 kHz, matrix: 128(PE) × 256, FOV: 18 cm, and slice thickness: 5 mm). Three different TE values were used for the temperature measurements: TE_1 = 17.2 ms, TE_2 = 18 ms and TE_3 = 19.8 ms. Temperature values obtained with our fat-suppressed rFOV sequence were compared to values obtained with the product FGRE sequence, using the same imaging parameters as employed for clinical temperature mapping applications at our institution. The experimental set-up was shown in Fig. 2 for illustration.

5. Results

5.1. Simulation results

Fig. 3 shows the temperature error for various TE values and field strengths B_0, in the presence of 20% fat (A_f/A_w = 20%) and an actual temperature rise of 10 °C. The phase modulation caused by fat creates an oscillation of the measured temperature around the true temperature value. Higher B_0 values lead to faster oscillations. Because fat has a shorter T_2^* value than water, the temperature deviation is attenuated for longer TE values.

Fig. 4a shows the dependence of the measured temperature error on fat percentage, for a fixed TE value of 10 ms at 3*T*, for different temperature changes. The measurement error does not necessarily increase monotonically with the fat percentage or the actual temperature rise. There is no single optimal TE value for accurate temperature measurement for objects with different fat contents. As seen in Fig. 4a, temperature errors tend to be small in all cases where fat content is low, confirming that the most effective solution to minimize the temperature measurement error may be to suppress the fat signals. The measured temperature deviations for different fat percentages are illustrated in Fig. 4b, when a fixed TE value of 10 ms is used at 3*T*. To keep the measurement error within 1 °C for practical clinical use, fat must be maintained within 5% or less (see green[1] curve in Fig. 4b). Thus, fat has to be suppressed by as much as 90% for very fatty tissues (with 50% fat component).

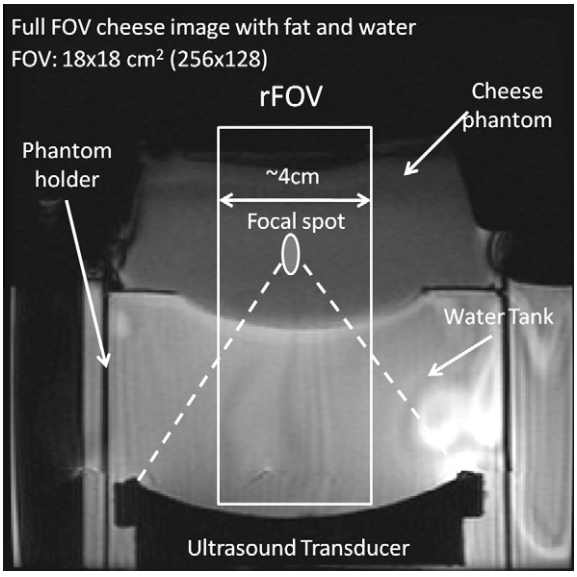

Fig. 2. The experimental setting for the rFOV temperature mapping in a cheese phantom.

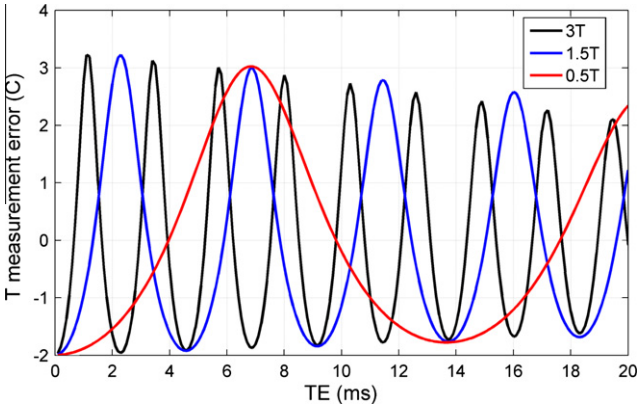

Fig. 3. Simulation of the measured temperature deviation obtained using the PRF model with different TE values. The simulation assumes the presence of 20% fat at various magnetic field strengths, B_0, and for a temperature rise of 10 °C.

5.2. Scan results

Fig. 5 shows excitation patterns obtained using the 11 × 1140 μs 2DRF pulse with fat suppression and rFOV, on a

[1] For interpretation of color in Fig. 4, the reader is referred to the web version of this article.

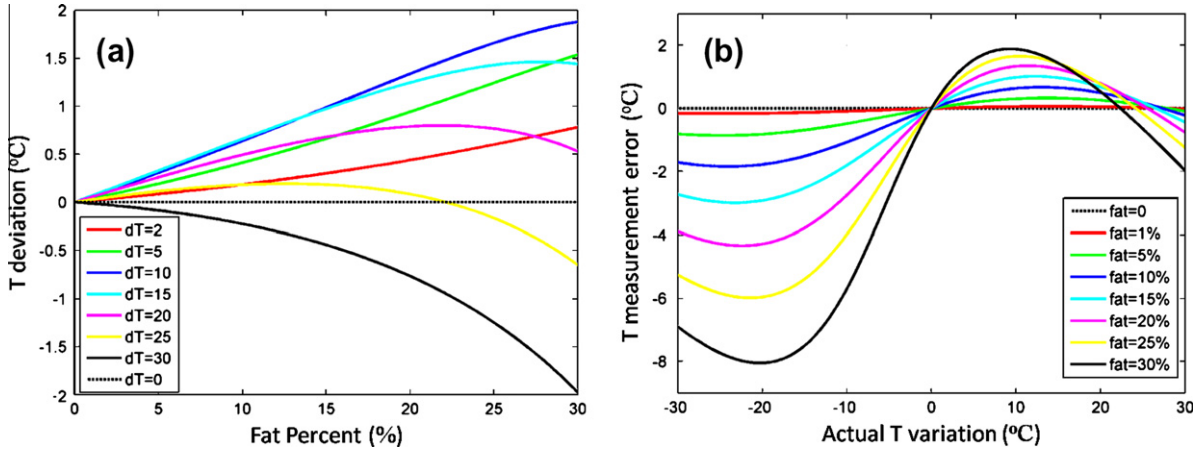

Fig. 4. (a) Dependence of the measured temperature error on the fat percentage for different temperature changes (dT). (b) The measured temperature deviations for various fat percentages. In order to keep measurement error within 1 °C for practical clinical use, the fat component must be less than 5%. For (a and b), TE = 10 ms and $B_0 = 3T$ are assumed.

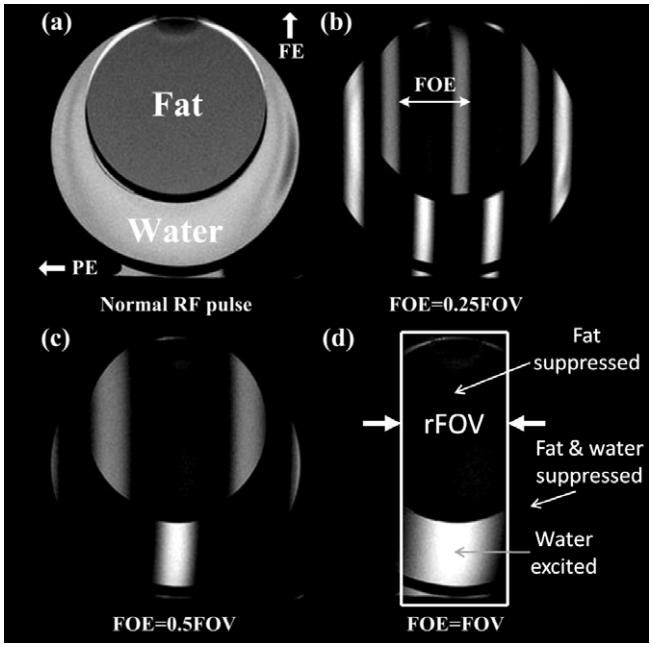

Fig. 5. Fat suppression and rFOV imaging in a phantom consisting of vegetable oil and water when using the 2DRF pulse. (a) The reference image produced by the normal FGRE sequence with the original slice-selective RF pulse. Note the chemical shift along the frequency encoding direction (vertical) due to the narrow receiver bandwidth of 8.06 KHz. (b–d) 2DRF pulse excitation profiles with different FOE values. The center of the water passband coincides with the center of the fat stopband to maximize the FOV reduction factor. In (d), only a fraction of water at the FOV center is excited, so rFOV imaging with fewer phase encodes can be applied to accelerate the acquisition without causing aliasing.

phantom consisting of vegetable oil and water, without heating. Fig. 5a is the reference image produced by the original FGRE sequence with a normal slice-selective RF pulse. Fig. 5b–d show the 2DRF excitations with different FOE values, where the center of the water passband coincides with the center of the fat stopband. By increasing the FOE, only the water in the central reduced-FOV region was excited and the fat in this region was suppressed (Fig. 5d). Outside of reduced-FOV region, neither fat nor water was excited at all. In this case, a fractional phase FOV could be selected to reduce the PE number and the scan time. By measuring the image intensity in the passband and stopband of fat, it is shown that fat was homogeneously suppressed by more than 90%. Theoretically, a maximum FOV reduction factor of 2.8 could be achieved by using this 2DRF pulse when $S = W_p + 2W_s$, where S is the maximum size of the scanned object along the phase encoding direction in the image FOV.

Fig. 6 shows the focal point (a 3×3 pixels square ROI) temperature measurement curves without and with 2DRF pulse excitation. The temperature measurements with the normal RF pulse excitation (black curves) featured a strong dependence on TE, despite identical FUS heating. As discussed, the presence of fat modulates the phase variation and causes significant measurement errors. The temperature rise peak was up to 6.87 (±0.69, standard deviation) °C for TE of 18 ms. In contrast, the temperature change peaks were 5.72(±0.54) °C and 3.96(±0.32) °C for TEs of 19.8 ms and 17.2 ms, respectively. Each temperature measurement took 5 s for a temporal resolution of 12 frames per minute (fpm). For comparison, consistent temperature curves (in blue) were obtained regardless of TE value for the measurements made using the 2DRF pulse excitation, with corresponding temperature peaks of 5.06(±0.37) °C, 5.13(±0.59) °C and 5.00(±0.35) °C for TE values of 17.2 ms, 18 ms and 19.8 ms, respectively. The red curve in Fig. 6 shows the temperature measurement curve obtained with the 2DRF excitation while applying an rFOV factor of 2.5. The temperature rise peak is measured as 5.24(±0.79) °C. Temporal resolution in this case was improved from 12 fpm to 28 fpm, without sacrificing spatial resolution or measurement consistency.

6. Discussion

As an alternative to the approach taken here, other fat suppression methods may be considered for temperature mapping, such as the use of a spectrally selective RF pulse or short tau inversion recovery (STIR) [23]. Compared to the proposed 2DRF excitation, the total duration of a spectrally selective pulse and the associated spoiler gradient is normally comparable with the duration of our 2DRF pulse. However, spectrally selective pulses excite the whole imaging volume without providing the option for reduced FOV imaging. In addition, a 2DRF pulse excitation is less sensitive to B_1 inhomogeneity. STIR uses an inversion pulse and achieves fat suppression by taking advantage of the shorter T_1 of fat as compared to that of water. The long inversion time (TI), however, is incompatible with the goal of improving the imaging speed. Furthermore, the image SNR is substantially reduced due to the T_1 relaxation of water. Dixon methods [24,25] and other related methods [26–28] use the phase information of images obtained

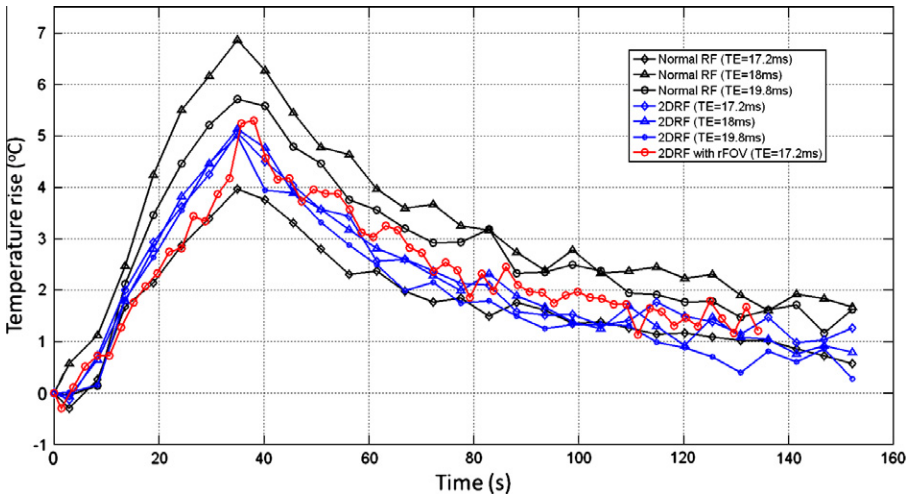

Fig. 6. The focal point temperature curves without and with 2DRF pulse excitation with identical FUS heating in a mixed fat–water phantom. The temperature measurements using a normal slice-selective RF pulse (black curves) show a strong dependence on TE value in spite of the identical sonication parameters used. The inconsistency of the temperature measurements is significantly improved due to the fat suppression using the 2DRF excitation (blue curves). By employing a fractional phase FOV factor of 0.4 for rFOV imaging (red curve), the temporal resolution was enhanced from 12 fpm to 28 fpm without a significant sacrifice in temperature accuracy. (For interpretation of the references to color in this figure legend, the reader is referred to the web version of this article.)

with different TEs to separate fat and water effectively. However, the multiple acquisitions (at least three) increase scan time, even when a multi-echo acquisition is used. The phase correction algorithm and the T_2^* decay effect between multi-echoes impose an increased computation load during reconstruction. Furthermore, this approach encounters difficulties whenever voxels containing only water or only fat are present [28].

Recently, an echo combination method has been proposed to reduce PRF thermometry errors from fat [29]. In the approach, three echoes are acquired and then combined into a single temperature map with predetermined weights to mitigate the temperature overestimation and underestimation at different TEs. However, the remaining error may still exceed 20% for a fat content of 30%, which might not be acceptable for temperature monitoring during thermal therapies [29]. Moreover, the weighting factors for the three acquisitions are very dependent on field strength and fat content, and accordingly, the echo combination is more of an empirical solution rather than a general one such as fat suppression. Also, the three-echo acquisition approach lengthens TR considerably, especially for situations when a low receiver bandwidth is used to increase SNR.

Since a relatively long TE comparable to T_2^* is often used to maximize the temperature-to-noise-ratio (TNR) in temperature mapping, the long duration of our 2DRF pulse supporting both fat suppression and rFOV imaging does not significantly reduce the image SNR or increase TR. One important advantage of rFOV imaging is that the number of phase encodes can be significantly reduced to accelerate imaging speed when a fractional FOV is excited by the 2DRF pulse.

The main drawback of the proposed approach is presumably its sensitivity to field inhomogeneities (e.g., B_0 inhomogeneity, susceptibility, and frequency shifts induced by heating itself). According to Eq. (7) and using the parameters from Fig. 5d (FOV = FOE = 34 cm and T_{sub} = 1140 μs), a B_0 shift of 1 ppm at 3T may cause a spatial shift as large as 5 cm. In practice, such shift might be caused by respiration and by the nearby presence of sonication equipment, for example. The best protection against spatial distortions of the excitation profile is to keep field inhomogeneities to a minimum, through careful shimming. Furthermore, in cases where the frequency shifts could be predicted, a careful calibration of the 2DRF pulse could alleviate any distortion [30].

A higher FOV reduction factor and hence higher temporal resolution might be achieved by further optimizing the 2DRF parameters, such as the number of sub-pulses, the sub-pulse duration and blip areas. The 2DRF excitation strategy described here is generally compatible with all pulse sequences being used for temperature mapping purposes, such as EPI sequences. By combining this method with SENSE [31] and UNFOLD [32], possible aliasing in the rFOV region could be effectively eliminated when an even shorter 2DRF pulse is used. Note that for a long 2DRF pulse such as the one in this study, no aliasing would be induced because neither fat nor water is excited outside of the rFOV region.To maximize the achievable rFOV factor and avoid the possible aliasing wrapped into the rFOV region, the 2DRF parameters and the imaging setting should be carefully adjusted. First of all, the focal point of the ultrasound is expected to be located in the center of FOV. As described in the theory section, the fat profile Δr must be shifted by $\Delta r \geqslant W_p$ for fat suppression. When Δr = 0.5FOE, the center of water passband coincides with the center of fat stopband precisely. For this purpose, the 2DRF sub-pulse duration was set as 1140 μs in this study at 3T according to Eq. (7). Theoretically, the more the sub-pulses, the higher ratio of stopband width (W_s) to passband width (W_p) so as the higher FOV reduction factor can be achieved. A sub-pulse number of eleven was applied in this study. A maximum FOV reduction factor of 2.8 could be achieved by using such a 2DRF pulse when the maximum size of the scanned subject along the phase encoding direction S equals to $W_p + 2W_s$, assumed that FOV is set equal to S. In other word, the minimum allowable rFOV size should be S/2.8. Otherwise, the side excitation within the subject may be wrapped into the rFOV region to contaminate the water-only image within rFOV.

In conclusion, a fast and accurate temperature mapping method using a 2DRF pulse enabling both fat suppression and rFOV was implemented. This technique is promising for real-time temperature monitoring of FUS thermal therapies in adipose organs.

Acknowledgment

This work is supported by NIH Grant U41RR019703.

References

[1] D.L. Parker, V. Smith, P. Sheldon, L.E. Crooks, L. Fussell, Temperature distribution measurements in two-dimensional NMR imaging, Med. Phys. 10 (1983) 321–325.

[2] R.J. Dickinson, A.S. Hall, A.J. Hind, I.R. Young, Measurement of changes in tissue temperature using MR imaging, J. Comput. Assist. Tomogr. 10 (1986) 468–472.
[3] J. Chen, B.L. Daniel, K.B. Pauly, Investigation of proton density for measuring tissue temperature, J. Magn. Reson. Imag. 23 (2006) 430–434.
[4] S.J. Graham, G.J. Stanisz, A. Kecojevic, M.J. Bronskill, R.M. Henkelman, Analysis of changes in MR properties of tissues after heat treatment, Magn. Reson. Med. 42 (1999) 1061–1071.
[5] D. Le Bihan, J. Delannoy, R.L. Levin, Temperature mapping with MR imaging of molecular diffusion: application to hyperthermia, Radiology 171 (1989) 853–857.
[6] Y. Ishihara, A. Calderon, H. Watanabe, K. Okamoto, Y. Suzuki, K. Kuroda, Y. Suzuki, A precise and fast temperature mapping using water proton chemical shift, Magn. Reson. Med. 34 (1995) 814–823.
[7] J. De Poorter, C. De Wagter, Y. De Deene, C. Thomsen, F. Stahlberg, E. Achten, Noninvasive MRI thermometry with the proton resonance frequency (PRF) method: in vivo results in human muscle, Magn. Reson. Med. 33 (1995) 74–81.
[8] W. Wlodarczyk, M. Hentschel, P. Wust, R. Noeske, N. Hosten, H. Rinneberg, R. Felix, Comparison of four magnetic resonance methods for mapping small temperature changes, Phys. Med. Biol. 44 (1999) 607–624.
[9] K. Kuroda, A.H. Chung, K. Hynynen, F.A. Jolesz, Calibration of water proton chemical shift with temperature for noninvasive temperature imaging during focused ultrasound surgery, J. Magn. Reson. Imag. 8 (1998) 175–181.
[10] R.D. Peters, R.S. Hinks, R.M. Henkelman, Ex vivo tissue-type independence in proton-resonance frequency shift MR thermometry, Magn. Reson. Med. 40 (1998) 454–459.
[11] K. Kuroda, K. Oshio, R.V. Mulkern, F.A. Jolesz, Optimization of chemical shift selective suppression of fat, Magn. Reson. Med. 40 (1998) 505–510.
[12] J.A. de Zwart, F.C. Vimeux, C. Delalande, P. Canioni, C.T. Moonen, Fast lipid-suppressed MR temperature mapping with echo-shifted gradient-echo imaging and spectral-spatial excitation, Magn. Reson. Med. 42 (1999) 53–59.
[13] C. Weidensteiner, B. Quesson, B. Caire-Gana, N. Kerioui, A. Rullier, H. Trillaud, C.T. Moonen, Real-time MR temperature mapping of rabbit liver in vivo during thermal ablation, Magn. Reson. Med. 50 (2003) 322–330.
[14] R.J. Stafford, J.D. Hazle, G.H. Glover, Monitoring of high-intensity focused ultrasound-induced temperature changes in vitro using an interleaved spiral acquisition, Magn. Reson. Med. 43 (2000) 909–912.
[15] K. Scheffler, Fast frequency mapping with balanced SSFP: theory and application to proton-resonance frequency shift thermometry, Magn. Reson. Med. 51 (2004) 1205–1211.
[16] C. Weidensteiner, N. Kerioui, B. Quesson, B.D. de Senneville, H. Trillaud, C.T. Moonen, Stability of real-time MR temperature mapping in healthy and diseased human liver, J. Magn. Reson. Imag. 19 (2004) 438–446.
[17] J.A. Bankson, R.J. Stafford, J.D. Hazle, Partially parallel imaging with phase-sensitive data: increased temporal resolution for magnetic resonance temperature imaging, Magn. Reson. Med. 53 (2005) 658–665.
[18] J. Yuan, B. Madore, L.P. Panych, Fat–water selective excitation in balanced steady-state free precession using short spatial-spectral RF pulses, J. Magn. Reson. (2010).
[19] C.H. Meyer, J.M. Pauly, A. Macovski, D.G. Nishimura, Simultaneous spatial and spectral selective excitation, Magn. Reson. Med. 15 (1990) 287–304.
[20] J. Yuan, B. Madore, L.P. Panych, Spatially varying fat–water excitation using short 2DRF pulses, Magn. Reson. Med. 63 (2010) 1092–1097.
[21] K. Kuroda, K. Oshio, A.H. Chung, K. Hynynen, F.A. Jolesz, Temperature mapping using the water proton chemical shift: a chemical shift selective phase mapping method, Magn. Reson. Med. 38 (1997) 845–851.
[22] J. Pauly, D. Nishimura, A. Macovski, A k-space analysis of small-tip-angle excitation, J. Magn. Reson. 81 (1989) 43–56.
[23] J.L. Fleckenstein, B.T. Archer, B.A. Barker, J.T. Vaughan, R.W. Parkey, R.M. Peshock, Fast short-tau inversion-recovery MR imaging, Radiology 179 (1991) 499–504.
[24] W.T. Dixon, Simple proton spectroscopic imaging, Radiology 153 (1984) 189–194.
[25] G.H. Glover, E. Schneider, Three-point Dixon technique for true water/fat decomposition with B_0 inhomogeneity correction, Magn. Reson. Med. 18 (1991) 371–383.
[26] Q.S. Xiang, L. An, Water–fat imaging with direct phase encoding, J. Magn. Reson. Imag. 7 (1997) 1002–1015.
[27] S.B. Reeder, Z. Wen, H. Yu, A.R. Pineda, G.E. Gold, M. Markl, N.J. Pelc, Multicoil Dixon chemical species separation with an iterative least-squares estimation method, Magn. Reson. Med. 51 (2004) 35–45.
[28] B.J. Soher, C. Wyatt, S.B. Reeder, J.R. MacFall, Noninvasive temperature mapping with MRI using chemical shift water–fat separation, Magn. Reson. Med. 63 (2010) 1238–1246.
[29] V. Rieke, K. Butts Pauly, Echo combination to reduce proton resonance frequency (PRF) thermometry errors from fat, J. Magn. Reson. Imag. 27 (2008) 673–677.
[30] M. Oelhafen, K.P. Pruessmann, S. Kozerke, P. Boesiger, Calibration of echo-planar 2D-selective RF excitation pulses, Magn. Reson. Med. 52 (2004) 1136–1145.
[31] K.P. Pruessmann, M. Weiger, M.B. Scheidegger, P. Boesiger, SENSE: sensitivity encoding for fast MRI, Magn. Reson. Med. 42 (1999) 952–962.
[32] B. Madore, G.H. Glover, N.J. Pelc, Unaliasing by fourier-encoding the overlaps using the temporal dimension (UNFOLD), applied to cardiac imaging and fMRI, Magn. Reson. Med. 42 (1999) 813–828.